Korean J. Chem. Eng., 37(10), 1786-1794 (2020)
DOI: 10.1007/s11814-020-0593-3

pISSN: 0256-1115
eISSN: 1975-7220

Preparation of nano-sized Mg-doped copper silicate materials using coal gangue as the raw material and its characterization for CO_2 adsorption

Yu Wu*,, Zhaojun Wu*,**, Kai Liu*,**, Fu Li*,**, Yujie Pang*,**, Jianbin Zhang*,**,†, and Huayan Si**,***,†**

*College of Chemical Engineering, Inner Mongolia University of Technology, Hohhot 010051, China
**Inner Mongolia Engineering Research Center for CO_2 Capture and Utilization, Hohhot 010051, China
***School of Materials Science and Engineering, Hebei Provincial Key Laboratory of Traffic Engineering materials, Shijiazhuang Tiedao University, Shijiazhuang 050043, China
(*Received 29 March 2020 • Revised 17 May 2020 • Accepted 27 May 2020*)

Abstract−This work presents a simple method for the preparation of the Mg-doped nanocomposite copper silicates (Mg_x-Cu_{1-x}-SiO_3) (x=0.25, 0.5, 0.75 and 0.9) using coal gangue waste as the silicon source for CO_2 capture at low temperature. The as-prepared Mg_x-Cu_{1-x}-SiO_3 was systemically characterized by scanning electron microscopy (SEM), Fourier-transform infrared spectroscopy (FTIR), X-ray powder diffraction (XRD), X-ray photoelectron spectroscopy (XPS) and Brunauer-Emmett-Teller surface area analysis (BET). The results suggest that all Mg_x-Cu_{1-x}-SiO_3 possess large surface areas, micropores and mesoporous structures composed of the agglomerates of small nanoparticles. They exhibit high CO_2 adsorption capacity at 298.15 K under 1 bar, and that of $Mg_{0.9}$-$Cu_{0.1}$-SiO_3 was the highest with the value of 16.73 cm^3/g. The Freundlich isotherm model fits the CO_2 adsorption isotherm well. Thermodynamic analysis indicates that the CO_2 adsorption on $Mg_{0.9}$-$Cu_{0.1}$-SiO_3 is exothermic ($\Delta H^o<0$), chaotic ($\Delta S^o<0$), and spontaneous ($\Delta G^o<0$). This work highlights the low-temperature adsorption behavior of silicate materials on CO_2, which can provide some research basis for the utilization of silica in coal gangue.

Keywords: Coal Gangue, Mg-doped Copper Silicate, CO_2, Adsorption, Thermodynamic Parameters

INTRODUCTION

Coal is the major energy source in China. The production and processing of coal have produced significant amounts solid coal gangue wastes concomitantly, usually accounting for 10-25% of the total weight of the coal [1,2]. So far, 700 million tons of coal gangue are piled up in China [3]. This massive accumulation of coal gangue has posed serious threats to environment. In addition to the land resources for the storage of these coal gangue wastes [4], the harmful gases emitted by their spontaneous combustion have caused serious air pollution [5] and the heavy metals and organic matter in coal gangue cause water pollution [6]. Therefore, the utilization of coal gangue is highly urgent and desired for both environmental and economic reasons. Alumina and silica in coal gangue are potential materials for waste valorization [7]. Gao et al. [8] prepared porous silica with the Si extracted from coal gangue for CO_2 capture. Qian et al. [9] synthesized Na-Al zeolites using coal gangue as the detergent builder. Xiao et al. [10] separated aluminum and silica from coal gangue for the preparation of alumina and SiC.

Excessive use of fossil fuels in industries has led to the emission of large amounts of CO_2 to the atmosphere, which is one of the major causes of the greenhouse effect [11,12]. Since the industrial revolution, the CO_2 concentration in the atmosphere has increased by ~40% [13] with a value of ~406 ppm in 2017 [14]. The over-emission of CO_2 has affected a variety of fields, such as marine biology, agriculture and economy [15]. Therefore, effectively reducing and controlling CO_2 emission is of great importance [16]. Currently, there are three major approaches to CO_2 capture: absorption, adsorption and membrane separation [17]. The adsorption approach has become the most attractive method due to its adaptable application conditions, low cost, low energy consumption and low corrosion. Various solid adsorbents have been developed for CO_2 removal, such as activated carbons [18,19], zeolites [20-22], metal-organic frameworks (MOFs) [23,24] and silicate materials [25]. Among these, metal silicate exhibits the most prospective application potential with its relatively high adsorption capacity, excellent cyclic stability and low cost raw materials [26]. Lithium silicate [27], magnesium silicate [28] and calcium silicate [29] are the most studied ones. They absorb CO_2 by the chemical reaction with CO_2 to form carbonates at high temperatures [30]. For higher CO_2 adsorption capacity, these metal silicates are usually doped with other metals. For example, Li_4SiO_4 is prone to agglomerate due to its small surface area [31], which significantly affects its CO_2 adsorption. Studies have shown that the doping of metal elements, such as Na [32], K [33], Al [34], V [34] and Fe [35], can improve the CO_2 adsorption performance of Li_4SiO_4 [36]. However, the physical CO_2 adsorption on metal silicates at low temperatures has been rarely reported.

A copper silicate with a specific surface area of 521.6 m^2/g and the CO_2 adsorption capacity of 10.59 cm^3/g has been previously reported [37]. And it also has been reported the CO_2 adsorption capacity of magnesium silicate can reach 14.97 cm^3/g. In the present work,

†To whom correspondence should be addressed.
E-mail: tadzhang@pku.edu.cn, sihuayan@stdu.edu.cn

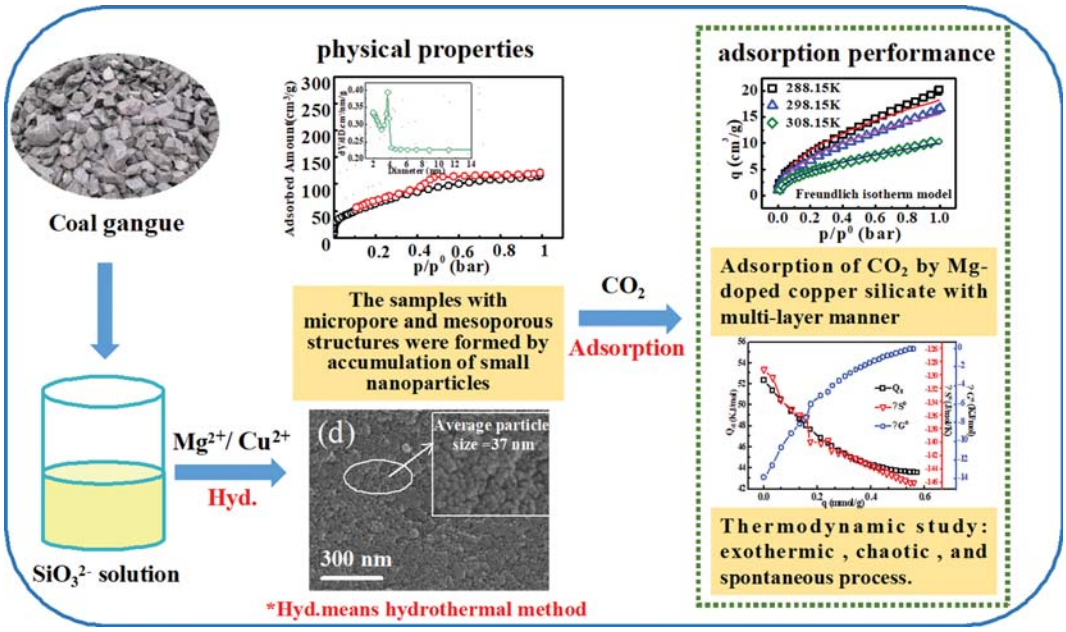

Fig. 1. Schematic illustration for the preparation and application of Mg_x-Cu_{1-x}-SiO_3 (x=0.25, 0.5, 0.75, and 0.9).

a new adsorbent for CO_2 capture at low temperature was prepared by doping Mg in the copper silicate prepared with coal gangue, aiming to explore the feasibility of utilizing coal gangue waste in a highly efficient, renewable and environment-friendly way. The Mg_x-Cu_{1-x}-SiO_3 (x=0.25, 0.5, 0.75 and 0.9) prepared with the silica leached from coal gangue was characterized by SEM, FTIR, XPS, XRD and BET. Their CO_2 adsorption performance was evaluated at 298.15 K under 1 bar and the corresponding adsorption isotherms and thermodynamics were determined. A general flow chart of the experiment is shown in Fig. 1. The CO_2 adsorption capacities of Mg_x-Cu_{1-x}-SiO_3, the Freundlich model fitting curves of the adsorptions at 288.15 K, 298.15 K, and 308.15 K, the CO_2 adsorption thermodynamics, and the morphology of $Mg_{0.9}$-$Cu_{0.1}$-SiO_3 were determined. Therefore, this work has provided a new strategy for the effective utilization of coal gangue wastes, and more importantly, created a new direction for the application of metal silicates to CO_2 capture.

EXPERIMENTAL

1. Materials

The coal gangue was supplied by Ordos Dongsheng Li Jiahao coal mine from Inner Mongolia province (China), and the main composition of coal gangue is shown in Table 1. NaOH and HCl were purchased from Yongsheng Fine Chemical Co (Tianjin, China), and $MgCl_2{\cdot}6H_2O$ was purchased from Sailboat Chemical Reagent Technology Co (Tianjin, China). $CuCl_2$ was obtained from Macklin Industry Inc. All chemical agents were analytical grade. CO_2 (99.999%) was provided by Beijing North oxygen special gas company.

2. Preparation of Mg-doped Copper Silicate

Mg_x-Cu_{1-x}-SiO_3 was prepared using the silicon liquor (SL) containing SiO_3^{2-} extracted from coal gangue. Coal gangue was calcined at 1,000 °C and extracted with 150 g/L NaOH at the m(calcined coal gangue)/m(NaOH) ratio of 15 at 100 °C for 2 h. The SiO_3^{2-} extraction rate was determined to be 77.69% [37]. To prepare Mg_x-Cu_{1-x}-SiO_3, the mixtures (50 mL) of Mg^{2+}/Cu^{2+} were prepared with 0.1 mol/L of magnesium chloride and 0.1 mol/L of copper chloride at the Mg^{2+}/Cu^{2+} molar ratios of 0.25/0.75, 0.5/0.5, 0.75/0.25 and 0.9/0.1 respectively, and poured into 50 mL 0.1 mol/L SL solutions. The pHs of solutions were then adjusted to 10 by adding concentrated HCl (10 M) dropwise. The final solutions were then heated to 140 °C for 10 hours. The products were washed with distilled water, filtered and dried to afford Mg_x-Cu_{1-x}-SiO_3 (x=0.25, 0.5, 0.75, and 0.9).

3. Characterization Methods

The crystalline structure of Mg_x-Cu_{1-x}-SiO_3 was performed by X-Ray diffraction (XRD) (Shimadzu, D/MAX-2500/PC) with Cu Kα radiation at 18 kV and 40 mA, and the samples were scanned between 5° and 75° 2θ at a scan rate of 30°·min^{-1}. Fourier transform infrared spectrophotometry (FTIR) of Mg_x-Cu_{1-x}-SiO_3 was recorded on a Bruker Tensor 27 FT-IR spectrometer between 500 and 4,000 cm^{-1} (Thermo-Fisher, NICOLETIS50). The XPS signals of $Mg_{0.9}$-$Cu_{0.1}$-SiO_3 were checked by XPS on a KRATOS Axis Ultra X-ray photoelectron spectrometer using twin anode MgKα/AlKα X-ray source. The morphology of Mg_x-Cu_{1-x}-SiO_3 was obtained by scanning electron microscope (SEM, S-3400N, Japan). The BET

Table 1. Primary chemical composition of coal gangue

Component	SiO_2	Al_2O_3	Na_2O	MgO	CaO	K_2O	Fe_2O_3	Others
Contents (wt%)	45	22	0.5	1	12	3	5	11.5

surface area of Mg_x-Cu_{1-x}-SiO_3 was estimated using 3H-2000PS2 analyzer apparatus and by obtaining N_2 adsorption-desorption isotherms; the pore size distribution was calculated according to the Barret Joyner Halenda (BJH) method [38].

4. CO_2 Adsorption Test

The CO_2 adsorption performance of the as-prepared Mg_x-Cu_{1-x}-SiO_3 was evaluated with a 3H-2000PS2 analyzer at 298.15 K under 1 bar. A schematic diagram of the experimental apparatus for the measurement of CO_2 is shown in Fig. S1. The adsorbent (1.0-1.5 g) was first packed into a round bottom glass tube, vacuum degassed at 120 °C for 120 minutes to remove the pre-adsorbed gas species, cooled to the test temperature and moved to the test position for the adsorption test. The adsorbed CO_2 was retrieved by heating the adsorbent at 120 °C.

5. Adsorption Isotherm

The CO_2 adsorption processes were analyzed according to the models of Langmuir and Freundlich isotherm. The linear form of Freundlich isotherm is as follows [39,40]:

$$q=kp^{1/n} \tag{1}$$

where k and n are the Freundlich constant that relates to the adsorption capacity, and q (cm^3/g) is the amount of CO_2 adsorbed at pressure p (bar).

The formula of Langmuir is described as follows [41,42]:

$$q=q_m\frac{bp}{1+bp} \tag{2}$$

where q_m is the maximum adsorption capacity of the adsorbent (cm^3/g), b is the Langmuir constant, and q and p are defined as Eq. (1).

6. Thermodynamics of Adsorption

The calculation of fundamental thermodynamic parameters could help better understand the adsorption process. The equivalent heat of adsorption Q_{st} (kJ/mol), the enthalpy change ΔH^o (kJ/mol), the entropy change ΔS^o (J/(mol·K)) and the Gibbs free energy change ΔG^o (kJ/mol) could be calculated from the following Eqs. (3)-(6) [43-46]:

$$\left[\frac{\partial \ln p}{\partial T}\right]=\frac{Q_{st}}{RT^2} \tag{3}$$

$$Q_{st}=-\Delta H^o \tag{4}$$

$$\Delta S^o=R\ln(p_o/p)-\frac{Q_{st}}{T} \tag{5}$$

$$\Delta G^o=\Delta H^o-T\Delta S^o \tag{6}$$

where p is the adsorption equilibrium pressure (bar), T is the temperature (K), and R is the ideal gas constant, 8.314 (J/(mol·K)). ΔH^o is variation of molecular enthalpy changes in the adsorption process; ΔS^o can be used to measure the disorder of system; and ΔG^o is calculated to determine the chemically thermodynamic process.

RESULTS AND DISCUSSION

1. Characterization Results.

1-1. SEM

The SEM images suggest that Mg_x-Cu_{1-x}-SiO_3 is composed of tightly agglomerated nano-particles (Fig. 2). Two kinds of agglomerates, the primary agglomerate of spherical particles with the sizes of 20-40 nm and the secondary agglomerate of the primary agglomerates, were observed. The secondary agglomerate might be formed due to the secondary agglomeration during the drying in furnace [47]. The energy spectra and elemental analysis indicate that Mg_x-Cu_{1-x}-SiO_3 is mainly composed of Si, Mg, Cu and O (Fig. S2 and

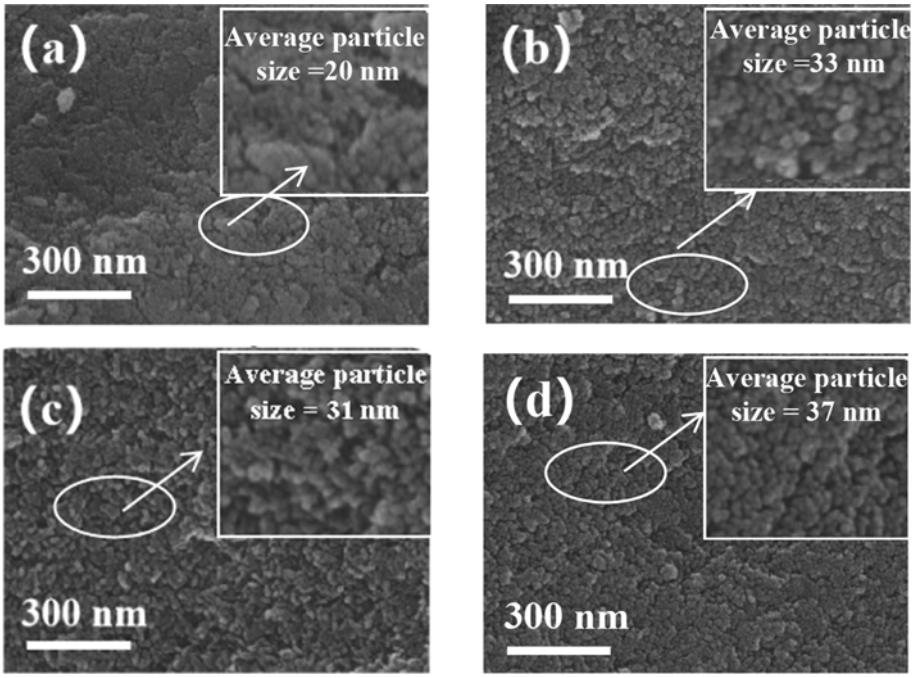

Fig. 2. SEM images of the $Mg_{0.25}$-$Mn_{0.75}$-SiO_3 (a), $Mg_{0.5}$-$Cu_{0.5}$-SiO_3 (b), $Mg_{0.75}$-$Cu_{0.25}$-SiO_3 (c), and $Mn_{0.9}$-$Cu_{0.1}$-SiO_3 (d).

Table 2. EDS analysis of the Mg_x-Cu_{1-x}-SiO_3 (x=0.25, 0.5, 0.75, and 0.9) materials

Mg_x-Cu_{1-x}-SiO_3	Element	O	Si	Cu	Mg
$Mg_{0.25}$-$Cu_{0.75}$-SiO_3	Wt%	47.20	22.54	27.08	3.17
	Atomic %	68.46	18.62	9.89	3.03
$Mg_{0.5}$-$Cu_{0.5}$-SiO_3	Wt%	55.73	21.79	16.82	5.67
	Atomic %	73.23	16.31	5.56	4.90
$Mg_{0.75}$-$Cu_{0.25}$-SiO_3	Wt%	46.61	26.85	12.09	14.44
	Atomic %	62.60	20.55	4.09	12.76
$Mg_{0.9}$-$Cu_{0.1}$-SiO_3	Wt%	35.59	35.73	10.39	18.28
	Atomic %	50.41	28.84	3.71	17.04

Table 2). Therefore, despite the complicated composition of coal gangue waste, only SiO_3^{2-} was extracted by the method developed in this work. In addition, as shown in the mapping diagrams (Fig. S3-S6), the elements are evenly distributed in Mg_x-Cu_{1-x}-SiO_3.

1-2. FT-IR

The Mg-doped copper silicates and copper silicate were further characterized by FT-IR. As shown in Fig. 3, all samples exhibited the bands at 3,443 cm^{-1} and 1,640 cm^{-1} due to the absorbed H_2O [48, 49]. The peak at 1,017 cm^{-1} was attributed to the stretching vibration of Si-O [50,51] and those at 768 cm^{-1} and 671 cm^{-1} were the characteristic absorption of SiO_3^{2-} [8], which indicated the existence of silicates and displayed that silicates can be synthesized with the SL as the silicon source.

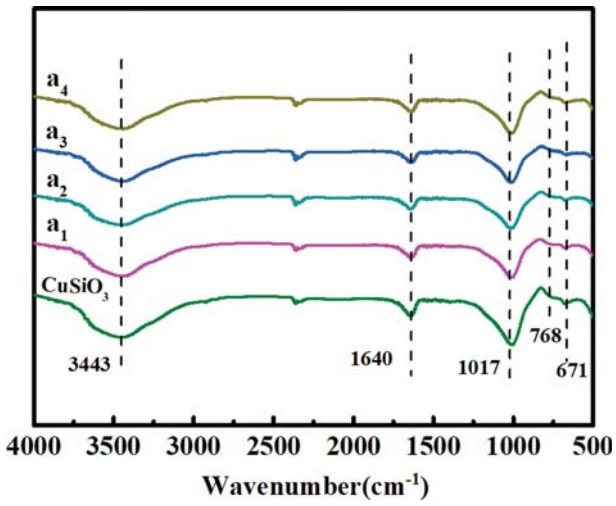

Fig. 3. FTIR spectra of Mg_x-Cu_{1-x}-SiO_3 (a_1: $Mg_{0.25}$-$Cu_{0.75}$-SiO_3; a_2: $Mg_{0.5}$-$Cu_{0.5}$-SiO_3; a_3: $Mg_{0.75}$-$Cu_{0.25}$-SiO_3; a_4: $Mn_{0.9}$-$Cu_{0.1}$-SiO_3).

1-3. XRD

Copper silicate exhibited three diffraction peaks at 2θ=31°, 57° and 63°, respectively [52] (Fig. S7). The doping resulted in three new peaks at 2θ=35°, 60° and 72°, which was attributed to $MgSiO_3$ [53]. The intensities of these new peaks increased with the increase of Mg content, indicating that the Mg element was successfully doped in copper silicate. The broad diffraction peak at 2θ=20° was at-

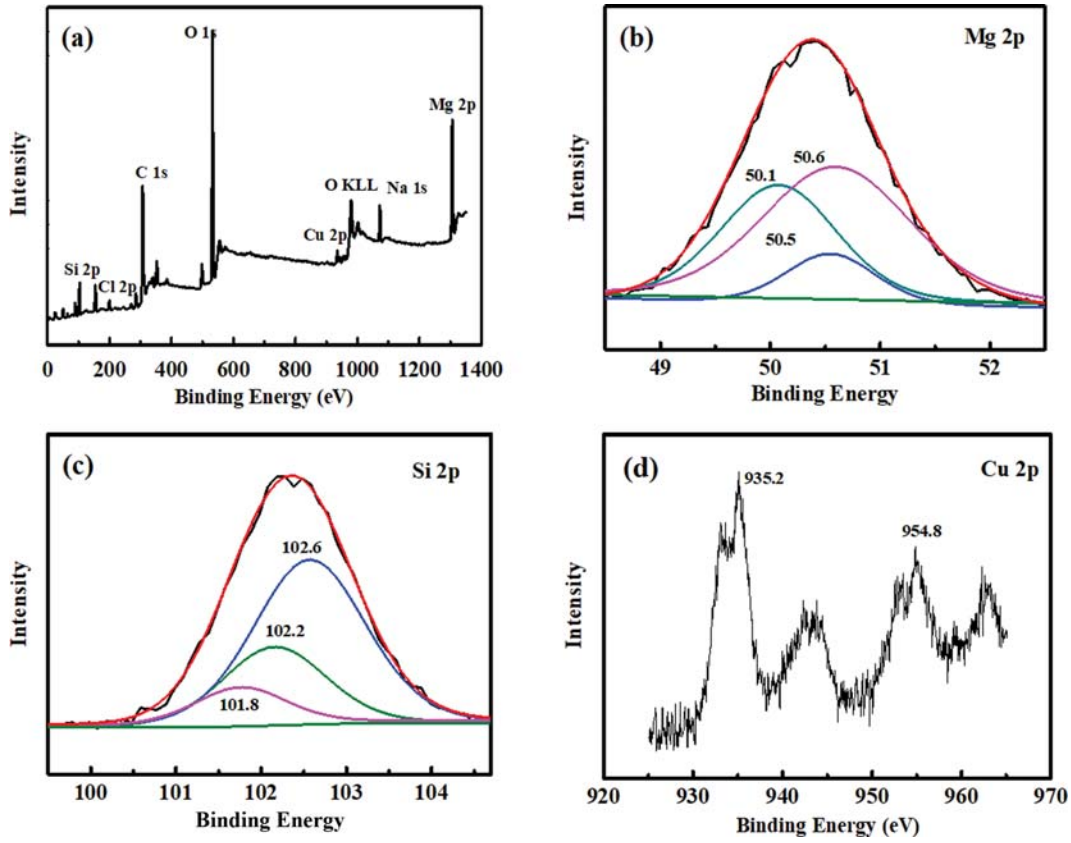

Fig. 4. XPS patterns of $Mg_{0.9}$-$Cu_{0.1}$-SiO_3: Overall spectra (a), Mg2p (b), Si2p (c), and Cu2p (d).

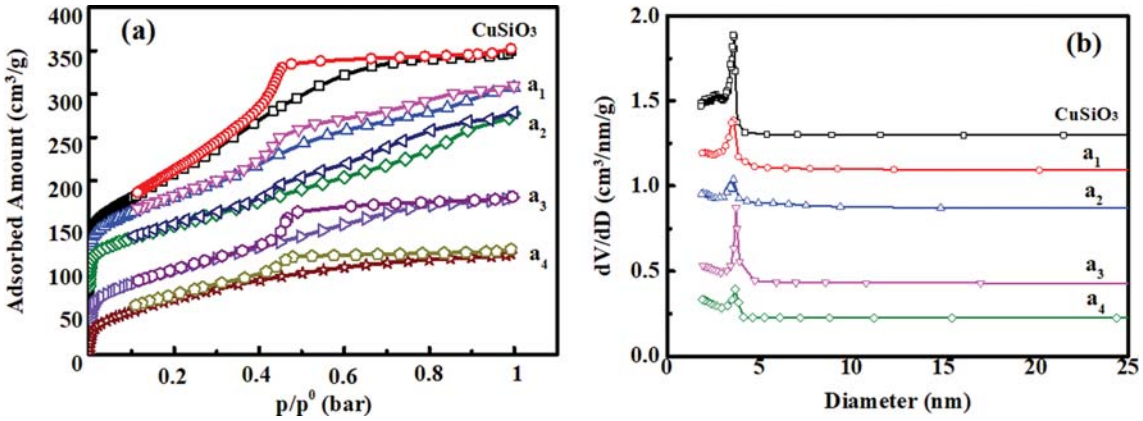

Fig. 5. N_2 adsorption-desorption isotherm (a) and BJH adsorption pore size distribution (b) of $CuSiO_3$, a_1: $Mg_{0.25}$-$Cu_{0.75}$-SiO_3, a_2: $Mg_{0.5}$-$Cu_{0.5}$-SiO_3, a_3: $Mg_{0.75}$-$Cu_{0.25}$-SiO_3, and a_4: $Mn_{0.9}$-$Cu_{0.1}$-SiO_3.

Table 3. Structural properties of the Mg_x-Cu_{1-x}-SiO_3 (x=0, 0.25, 0.5, 0.75, and 0.9) materials and CO_2 adsorption at 298.15 K and 1 bar

Materials	BET specific surface area (m^2/g)	Pore volume (mL/g)	Average pore size (nm)	CO_2 uptake (cm^3/g)
$CuSiO_3$	521.6	0.43	3.31	10.59
$Mg_{0.25}$-$Cu_{0.75}$-SiO_3	333.4	0.40	3.55	5.90
$Mg_{0.5}$-$Cu_{0.5}$-SiO_3	275.8	0.36	4.01	7.14
$Mg_{0.75}$-$Cu_{0.25}$-SiO_3	310.6	0.29	3.27	9.41
$Mg_{0.9}$-$Cu_{0.1}$-SiO_3	271.9	0.21	2.97	16.73

tributed to SiO_2 or SiO_3^{2-}. The broad diffraction peaks of the Mg-doped copper silicates suggest their crystalline sizes are small [54-57].

1-4. XPS

XPS was used to determine the oxidation states of magnesium and copper. Mg, Cu, O, Si, Cl, Na and C were found in $Mg_{0.9}$-$Cu_{0.1}$-SiO_3 (Fig. 4(a)). The Cl^- is from the chloride in coal gangue and the Na^+ derives from the SL. The peaks at 50.1 eV, 50.5 eV and 50.6 eV can be assigned to the Mg2p of $Mg(OH)_2$, MgO and Si-O-Mg (Fig. 4(b)). The Si2p peaks centered at 101.8 eV, 102.2 eV and 102.6 eV are corresponding to the Si in Si-O-Cu, Si-O-Mg and Si-O-Si, respectively (Fig. 4(c)). $Cu2p_{3/2}$ and $Cu2p_{1/2}$ were found at 935.2 and 954.8 eV, respectively, indicating that Cu species were in the form of Cu^{2+} [58]. Based on these results, it can be concluded that magnesium and copper are in the form of Mg^{2+} and Cu^{2+} in the Mg-doped copper silicate.

1-5. N_2 Adsorption-desorption Isotherms

Fig. 5 shows the N_2 adsorption/desorption isotherm curves and BJH adsorption pore size distributions of the Mg_x-Cu_{1-x}-SiO_3 (x= 0.25, 0.5, 0.75, and 0.9). The N_2 adsorption-desorption isotherms can be considered as the type IV isotherm with the prominent feature of mesoporous materials of $CuSiO_3$ [59]. a_3 and a_4 showed H2 hysteresis loops in the range of $0.4<p/p^o<0.8$ [60], indicating they were mesoporous structures with cage-like pores [61]. $CuSiOa_1$ and $CuSiOa_2$ exhibited H2 hysteresis loops in the range of $0.4<p/p^o<0.9$, suggesting that their pores were lit-like [61]. The N_2 adsorption increased sharply at low relative pressures, indicating the presence of micropores in the materials [62]. The pore sizes of all samples are mainly distributed in the range of 2-20 nm, and thus they are mesoporous structures. The BET specific surface area and pore volume of copper silicate were determined to be 521.6 m^2/g and 0.43 cm^3/g, respectively (Table 3), higher than those of Mg_x-Cu_{1-x}-SiO_3, indicating that the doped Mg occupied the pores of copper silicate. However, the specific surface areas of all Mg_x-Cu_{1-x}-SiO_3 were still higher than those of other silicate materials, such as copper silicate nanospheres-TA (10-14 m^2/g) [52].

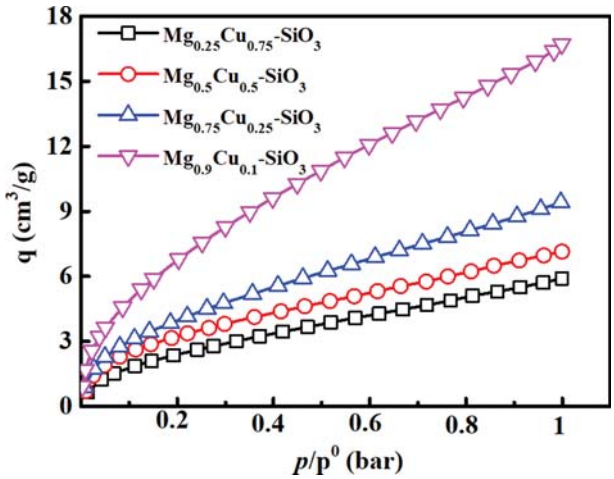

Fig. 6. CO_2 adsorption capacity on the surface of $Mg_{0.25}$-$Cu_{0.75}$-SiO_3, $Mg_{0.5}$-$Cu_{0.5}$-SiO_3, $Mg_{0.75}$-$Cu_{0.25}$-SiO_3, and $Mg_{0.9}$-$Cu_{0.1}$-SiO_3 materials.

2. CO_2 Adsorption

The Mg_x-Cu_{1-x}-SiO_3 prepared at different mass ratios of Mg to Cu were tested for CO_2 adsorption at 298.15 K under 1 bar. As shown in Fig. 6, the CO_2 adsorption increases with the increase of pressure and $Mg_{0.9}$-$Cu_{0.1}$-SiO_3 exhibits the highest CO_2 adsorption capacity (16.73 cm^3/g) (Fig. 6). As listed in Table 3, the BET specific surface area and pore volume of $Mg_{0.9}$-$Cu_{0.1}$-SiO_3 are the smallest. Therefore, there is no significant correlation between the specific surface area and the CO_2 adsorption capacity of the Mg_x-Cu_{1-x}-SiO_3. It can be explained that a large amount of hydroxyl groups on the silicate surface can form hydrogen bonds with CO_2 to capture CO_2. Therefore, the hydroxyl groups of silicate and the porous structure are the major contributors to the CO_2 adsorption. The CO_2 adsorption capacity initially decreased with the increase of the amount of Mg doped in $CuSiO_3$ because the doped Mg occupied the pores and reduced the specific surface area of $CuSiO_3$ for the adsorption. Further increasing the amount of doped Mg significantly increased the amount of hydroxyl groups, and thus increased the CO_2 adsorption capacity. In the previous work, we determined the CO_2 adsorption capacity of $MgSiO_3$ to be 14.973 cm^3/g, lower than that of $Mg_{0.9}$-$Cu_{0.1}$-SiO_3. Therefore, there is a synergistic effect between the silicates on the CO_2 adsorption. Table 4 lists the CO_2 adsorption capacity of other CO_2 adsorbents, including M-SiO_2 [25], copper silicate nanospheres [52], MOF-177 [52], and MCM-41 [67] under the pressure of 1 bar for comparison purpose. It is clear that $Mg_{0.9}$-$Cu_{0.1}$-SiO_3 exhibits a relatively high CO_2 adsorption capacity. The influence of temperature on the CO_2 adsorption capacity of $Mg_{0.9}$-$Cu_{0.1}$-SiO_3 was investigated in the range from 288.15 K to 308.15 K. As shown in Fig. 7, the CO_2 adsorption capac-

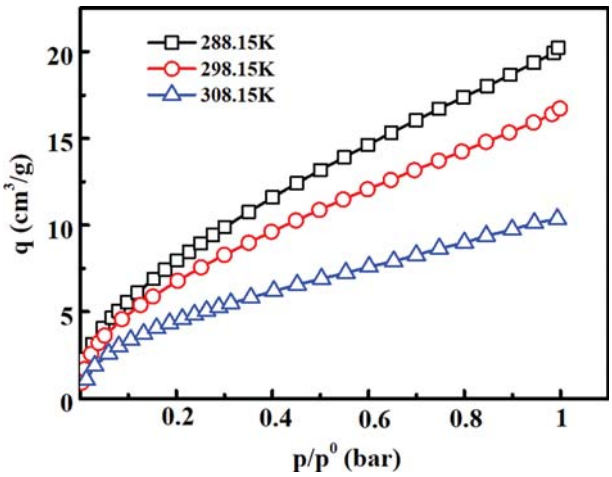

Fig. 7. CO_2 adsorption capacity on the surface of $Mg_{0.9}$-$Cu_{0.1}$-SiO_3 material at 288.15 K, 298.15 K, and 308.15 K.

Table 4. CO_2 adsorption capacities of various materials

Materials	T (K)	P (bar)	CO_2 uptake (cm^3/g)	Refs.
M-SiO_2	298.15	1	4.89	[25]
EDA-M-SiO_2	298.15	1	42.51	[25]
PEI-MSP-0.32	298.15	1	63.13	[62]
Copper silicate nanospheres	298.15	1	10.55	[51]
Copper silicate nanospheres-TA	303.15	1	24.38	[51]
C-PSM	298.15	1	4.59	[63]
MOF-177	313.15	1	14.56	[64]
SiO_2-PAA(3000)-PEI(10000)	313.15	1	85.12	[65]
MCM-41	318.15	1	1.57	[66]
$Mg_{0.9}$-$Cu_{0.1}$-SiO_3	298.15	1	16.73	This work

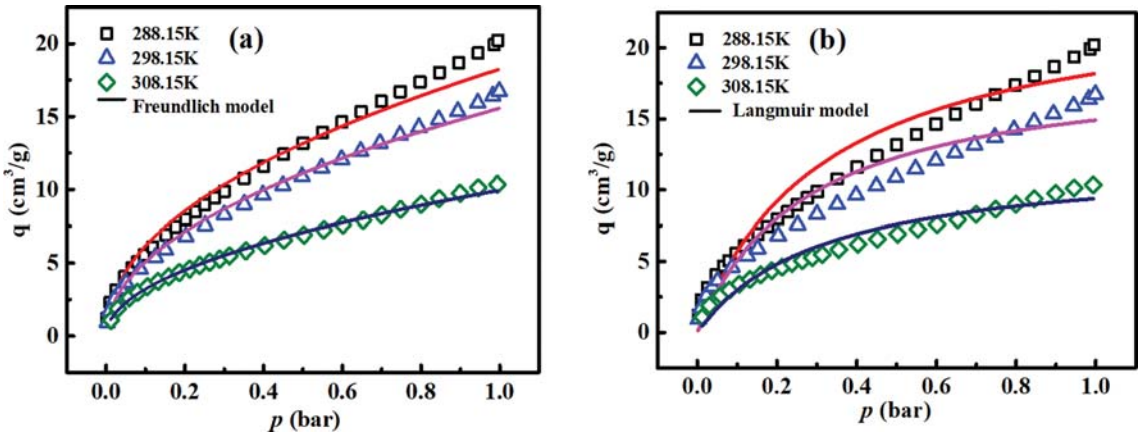

Fig. 8. Fitting of CO_2 adsorption isotherms plots Freundlich model (a) and Langmuir model (b) on the surface of $Mg_{0.9}$-$Cu_{0.1}$-SiO_3 material at 288.15 K, 298.15 K, and 308.15 K.

Table 5. Freundlich and Langmuir parameters for CO_2 adsorption on the $Mg_{0.9}$-$Cu_{0.1}$-SiO_3 material

Sample	T(K)	Freundlich			Langmuir		
		k	n	R^2	q_m (cm^3/g)	b (bar^{-1})	R^2
$Mg_{0.9}$-$Cu_{0.1}$-SiO_3	288.15	18.25	2.12	0.987	24.04	3.11	0.902
	298.15	15.57	2.06	0.997	18.98	3.67	0.915
	308.15	9.95	2.04	0.997	12.33	3.19	0.934

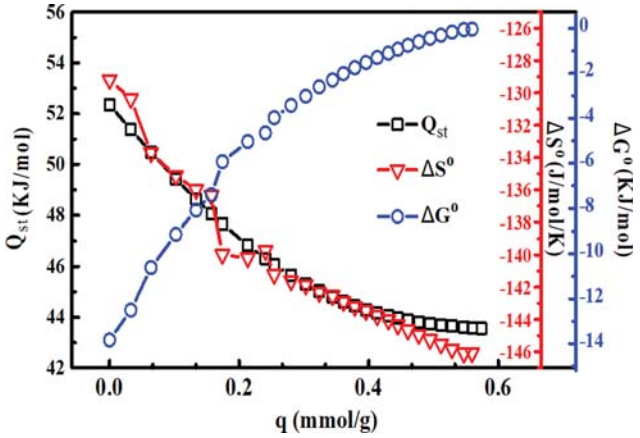

Fig. 9. Thermodynamic plots for CO_2 adsorption on the surface of $Mg_{0.9}$-$Cu_{0.1}$-SiO_3 material.

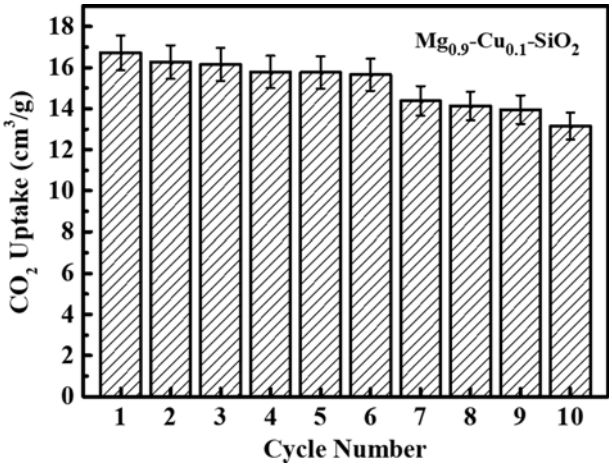

Fig. 10. Ten CO_2 adsorption/desorption cycles on the surface of $Mg_{0.9}$-$Cu_{0.1}$-SiO_3 materials.

ity of $Mg_{0.9}$-$Cu_{0.1}$-SiO_3 decreases gradually with the increase of temperature, suggesting that the CO_2 adsorption on $Mg_{0.9}$-$Cu_{0.1}$-SiO_3 is a typical physical adsorption.

3. Adsorption Isotherms

To further understand the CO_2 adsorption process of Mg_x-Cu_{1-x}-SiO_3, $Mg_{0.9}$-$Cu_{0.1}$-SiO_3 with the highest CO_2 adsorption capacity was tested as an example. The adsorption isotherms at different temperatures were fitted with the Langmuir and Freundlich adsorption models. Fig. 8 shows the fitted adsorption isotherm curves and Table 5 lists the adsorption parameters. It is clear that the Freundlich adsorption model fits the CO_2 adsorption of $Mg_{0.9}$-$Cu_{0.1}$-SiO_3 better with higher correlation coefficients (R^2). Based on these results, it can be concluded that the CO_2 adsorption on $Mg_{0.9}$-$Cu_{0.1}$-SiO_3 is multi-layer heterogeneous adsorption [68].

4. Adsorption Thermodynamics

The adsorption thermodynamic parameters including Q_{st}, ΔH^o, ΔS^o and ΔG^o can be used to determine the type of adsorption and the heterogeneity of the surface of adsorbent [69]. As shown in Fig. 9, the Q_{st} of $Mg_{0.9}$-$Cu_{0.1}$-SiO_3 decreases with the increase of the amount of adsorbed CO_2 (q), indicating that the material surface is heterogeneous with the adsorption sites of different energies [70]. In the early adsorption stage, the CO_2 molecules preferentially occupy the adsorption sites with higher energies, which requires lower activation energies and thus results in higher Q_{st}. With the progress of adsorption, the adsorption sites with higher energies are saturated, and the CO_2 molecules can only interact with the adsorption sites with lower energies, which requires higher activation energies. Q_{st} is then gradually decreased [68]. $Q_{st}>0$ and the $\Delta H^o<0$ indicate that the CO_2 adsorption process is exothermic [71]. The entropy change (ΔS^o) also decreases with the increase of q, and $\Delta S^o<0$. It can be explained that the surface of $Mg_{0.9}$-$Cu_{0.1}$-SiO_3 is gradually occupied by CO_2 during the adsorption. The CO_2 molecules are transferred from the three-dimensional moving range to the two-dimensional space of the $Mg_{0.9}$-$Cu_{0.1}$-SiO_3 surface, which reduces the chaos and thus results in decrease in entropy [72]. In addition, the Gibbs free energy change, ΔG^o, decreases with the increase of q, and $\Delta G^o<0$, indicating that the CO_2 adsorption of $Mg_{0.9}$-$Cu_{0.1}$-SiO_3 is a spontaneous process [73]. In all, the CO_2 adsorption on Mg_x-Cu_{1-x}-SiO_3 is an exothermic, entropy reduced and spontaneous process.

5. Regeneration

Regenerability is an imperative parameter to evaluate an adsorbent. Fig. 10 shows the CO_2 adsorption (T=298.15 K) and desorption (T=393.15 K) cyclability of $Mg_{0.9}$-$Cu_{0.1}$-SiO_3. The CO_2 adsorption capacity of $Mg_{0.9}$-$Cu_{0.1}$-SiO_3 decreased by 21% after ten adsorption-desorption cycles, which was mainly caused by the loss of -OH group as heated at 393.15 K during desorption. Therefore, $Mg_{0.9}$-$Cu_{0.1}$-SiO_3 possesses good cyclic regenerability.

CONCLUSIONS

A series of Mg_x-Cu_{1-x}-SiO_3 adsorbents were prepared by hydrothermal method using coal gangue as the silicon source. The characterization results suggest that adsorbents possess very large specific surface areas and rich pore structure, so silicate materials show typical physical adsorption of CO_2 at low temperature, and the adsorption performance is excellent. This work has not only provided a new strategy for the utilization of coal gangue waste, but also created a new research direction of the CO_2 capture with com-

posite silicates at low temperature.

ACKNOWLEDGEMENTS

This work was supported by the National Natural Science Foundation of China (Project No. 21466028), the Inner Mongolia Science and Technology Key Projects, the Program for Grassland Excellent Talents of Inner Mongolia Autonomous Region, and training plan of academic backbone in youth of Inner Mongolia University of Technology.

SUPPORTING INFORMATION

Additional information as noted in the text. This information is available via the Internet at http://www.springer.com/chemistry/journal/11814.

REFERENCES

1. C. Yi, H. Q. Ma, H. G. Zhu, Z. C. Dong, Z. J. Su, Y. T. Zhang and Z. Chu, *J. Build. Mater.*, **20**, 134 (2017).
2. Y. J. Li, Y. Xing, X. Zhang and X. P. Yan, *J. China Coal Soc.*, **38**, 1215 (2013).
3. C. Yi, H. Q. Ma, H. Y. Chen, J. X. Wang, J. Shi, Z. H. Li and M. K. Yu, *Constr. Build. Mater.*, **187**, 318 (2018).
4. C. C. Zhou, G. J. Liu, D. Wu, T. Fang, R. Wang and X. Fan, *Chemosphere*, **95**, 193 (2014).
5. Y. Tang and H. Wang, *Powder Technol.*, **323**, 486 (2018).
6. L. Zhou, H. J. Zhou, Y. X. Hu, S. Yan and J. L. Yang, *J. Environ. Manage.*, **234**, 245 (2019).
7. J. Geng, M. Zhou, T. Zhang, W. Wang, T. Wang, X. Zhou, X. Wang and H. Hou, *Mater. Struct.*, **50**, 5 (2017).
8. Y. J. Gao, H. Y. Huang, W. J. Tang, X. Y. Liu, X. Y. Yang and J. B. Zhang, *Micropor. Mesopor. Mater.*, **217**, 210 (2015).
9. T. T. Qian and J. H. Li, *Adv. Powder Technol.*, **26**, 98 (2015).
10. J. Xiao, F. C. Li, Q. F. Zhong, H. G. Bao, B. J. Wang, J. D. Huang and Y. B. Zhang, *Hydrometallurgy*, **155**, 118 (2015).
11. P. Jamrunroj, S. Wongsakulphasatch, A. Maneedaeng, C. K. Cheng and S. Assabumrungrat, *Powder Technol.*, **344**, 208 (2019).
12. O. Rahmani, R. Junin, M. Tyrer and R. Mohsin, *Energy Fuel*, **28**, 5953 (2014).
13. A. Sacco, *J. CO_2 Util.*, **27**, 22 (2018).
14. S. K. Kaliyavaradhan and T. C. Ling, *J. CO_2 Util.*, **20**, 234 (2017).
15. S. X. Wang, R. J. Farrauto, S. Karp, J. H. Jeona and T. Erik, *J. CO_2 Util.*, **27**, 390 (2018).
16. A. Álvarez, A. Bansode, A. Urakawa, A. V. Bavykina, T. A. Wezendonk, M. Makkee, J. Gascon and F. Kapteijn, *Chem. Rev.*, **117**, 9804 (2017).
17. H. Wu, L. Gao, H. Jin and S. Li, *Appl. Energy*, **203**, 571 (2017).
18. A. E. Creamer and B. Gao, *Environ. Sci. Technol.*, **50**, 7276 (2016).
19. D. Li, J. Zhou, Z. Zhang, L. Li, Y. Tian, Y. Lu, Y. Qiao, J. Li and L. Wen, *Carbon*, **114**, 496 (2017).
20. S. J. Chen, M. Zhu, Y. Fu, Y. X. Huang, Z. C. Tao and W. L. Li, *Appl. Energy*, **191**, 87 (2017).
21. K. Yoshihiro, S. Marie and E. Akira, *Micropor. Mesopor. Mater.*, **219**, 125 (2016).
22. E. Kim, S. Hong, E. Jang, J. H. Lee, J. C. Kim, N. Choi, C. H. Cho, J. Nam, S. K. Kwak, A. C. K. Yip and J. Choi, *J. Mater. Chem. A*, **5**, 11246 (2017).
23. Y. Belmabkhout, V. Guillerm and M. Eddaoudi, *Chem. Eng. J.*, **296**, 386 (2016).
24. S. Nandi, S. Haldar, D. Chakraborty and R. Vaidhyanathan, *J. Mater. Chem. A*, **5**, 535 (2017).
25. H. Du, L. Ma, X. Y. Liu, F. Zhang, X. Y. Yang, Y. Wu and J. B. Zhang, *Energy Fuel*, **32**, 5374 (2018).
26. S. C. Lee, M. J. Kim, Y. M. Kwon, H. J. Chae, M. S. Cho, Y. K. Park, H. M. Seo and J. C. Kim, *Sep. Purif. Technol.*, **120**, 214 (2019).
27. K. Essaki, M. Kato and H. Uemoto, *J. Mater. Sci.*, **21**, 5017 (2005).
28. J. J. Li, M. Hitch, I. M. Power and Y. Y. Pan, *Minerals*, **8**, 147 (2018).
29. J. J. Li and M. Hitch, *Miner. Eng.*, **128**, 69 (2018).
30. Y. C. Hu, W. Q. Liu, Y. D. Yang, M. Y. Qua and H. L. Li, *Chem. Eng. J.*, **359**, 604 (2019).
31. H. Xu, W. Cheng, X. Jin, G. Wang, H. Lu and H. Wang, *Ind. Eng. Chem. Res.*, **52**, 1886 (2013).
32. M. Seggiani, M. Puccini and S. Vitolo, *Int. J. Greenh. Gas. Control*, **17**, 25 (2013).
33. S. Zhang, Q. Zhang, H. Wang, Y. Ni and Z. Zhu, *Int. J. Hydrogen Energy*, **39**, 17913 (2014).
34. J. Ortiz-Landeros, C. Gomez-Yanez, L. M. Palacios-Romero, E. Lima and H. Pfeiffer, *J. Phys. Chem. A*, **116**, 3163 (2012).
35. C. Gauer and W. Heschel, *J. Mater. Sci.*, **41**, 2405 (2006).
36. X. X. Chen, Z. Xiong, Y. D. Qin, B. B. Gong, C. Tian, Y. C. Zhao, J. Y. Zhang and C. G. Zheng, *Int. J. Hydrogen Energy*, **41**, 13077 (2016).
37. Y. Wu, H. Du, Y. J. Gao, X. Y. Liu, T. Y. Yang, L. Zhao, X. Q. Yue, S. Zhang and J. B. Zhang, *Fuel*, **258**, 116192 (2019).
38. L. D. Gelb and K. E. Gubbins, *Langmuir*, **15**, 305 (1999).
39. M. F. Freundlich, *J. Phys. Chem.*, **57**, 355 (1906).
40. R. Thiruvenkatachari, S. Su, H. An and X. X. Yu, *Prog. Energ. Combust.*, **35**, 438 (2009).
41. M. Moradi, R. Karimzadeh and E. S. Moosavi, *Fuel*, **217**, 467 (2018).
42. Z. H. Ye, D. Chen, Z. J. Pan, G. Q. Zhang, Y. Xia and X. Ding, *J. Nat. Gas. Sci. Eng.*, **31**, 658 (2016).
43. P. Ammendola, F. Raganati and R. Chirone, *Chem. Eng. J.*, **322**, 302 (2017).
44. L. Hauchhum and P. Mahanta, *Int. J. Energy Environ. Eng.*, **5**, 349 (2014).
45. F. Raganati, M. Alfe, V. Gargiulo, R. Chirone and P. Ammendola, *Chem. Eng. Res. Des.*, **134**, 540 (2018).
46. V. K. Singh and E. A. Kumar, *Mater. Today*, **5**, 23033 (2018).
47. M. Dietemann, F. Baillon, F. Espitalier, R. Calvet, P. Accart, S. D. Confetto and M. Greenhill-Hooper, *Chem. Eng. J.*, **215-216**, 658 (2013).
48. S. T. Oyama and Y. K. Lee, *J. Catal.*, **258**, 393 (2008).
49. H. Y. Wang, Y. Y. Wang, X. Bai, H. Yang, J. P. Han, N. Lun, Y. X. Qi and Y. J. Bai, *RSC Adv.*, **6**, 105771 (2016).
50. Y. Zhang, Y. W. Li, Y. J. Dai, J. Liu and Y. B. Xu, *Ceram. Int.*, **44**, 6626 (2018).
51. Y. Zhang, Y. W. Li and Y. J. Dai, *Ceram. Int.*, **44**, 21365 (2018).
52. Y. P. Ren, R. Y. Ding, H. R. Yue, S. Y. Tang, C. J. Liu, J. B. Zhao, W. Lin and B. Liang, *Appl. Energy*, **198**, 250 (2017).
53. D. Nied, K. E. Rasmussen, E. L'Hopital, J. Skibsted and B. Lothen-

bach, *Cem. Concr. Res.*, **79**, 323 (2016).
54. H. Borchert, E. V. Shevchenko, A. Robert, I. Mekis, A. Kornowski, G. Grubel and H. Weller, *Langmuir*, **21**, 1931 (2005).
55. T. Li, A. J. Senesi and B. Lee, *Chem. Rev.*, **116**, 11128 (2016).
56. H. H. Liu, H. L. Zhang, H. B. Xu, T. P. Lou, Z. T. Sui and Y. Zhang, *Nanoscale*, **10**, 5246 (2018).
57. H. H. Liu, H. L. Zhang, Y. Y. Hu, H. B. Xu, T. P. Lou, Z. T. Sui and Y. Zhang, *J. Alloy Compd.*, **778**, 803 (2019).
58. L. S. Roselin and H. W. Chiu, *J. Saudi. Chem. Soc.*, **22**, 692 (2018).
59. J. J. Yuan, P. X. Zhu, D. Noda and R. H. Jin, *Beilstein J. Nanotechnol.*, **4**, 793 (2013).
60. S. Rahmani, M. Rezaei and F. Meshkani, *J. Ind. Eng. Chem.*, **20**, 1346 (2014).
61. C. Gunathilake, R. S. Dassanayake, N. Abidi and M. Jaroniec, *J. Mater. Chem. A*, **4**, 4808 (2016).
62. B. Ghods, M. Rezaei and F. Meshkani, *Ceram. Int.*, **42**, 6883 (2016).
63. W. Klinthong, C. H. Huang and C. S. Tan, *Ind. Eng. Chem. Res.*, **55**, 6481 (2016).
64. X. Y. Liu, X. Y. Yang, H. Du, Y. Wu, X. S. Zhang and J. B. Zhang, *Powder Technol.*, **333**, 138 (2018).
65. J. A. Mason, K. Sumida, Z. R. Herm, R. Krishna and J. R. Long, *Energy Environ. Sci.*, **4**, 3030 (2011).
66. Y. H. Du, Z. J. Du, W. Zou, H. Q. Li, J. G. Mi and C. Zhang, *J. Colloid Interface Sci.*, **409**, 123 (2013).
67. P. López-Aranguren, S. Builes, J. Fraile, L. F. Vega and C. Domingo, *Ind. Eng. Chem. Res.*, **53**, 15611 (2014).
68. Y. N. Zheng, Q. Z. Li, C. C. Yuan, Q. L. Tao, Y. Zhao, G. Y. Zhang, J. F. Liu and G. Qi, *Fuel*, **230**, 172 (2018).
69. L. Chen, L. Zuo, Z. X. Jiang, S. Jiang, K. Y. Liu, J. Q. Tan and L. C. Zhang, *Chem. Eng. J.*, **361**, 559 (2019).
70. B. J. Schindler and M. D. LeVan, *Carbon*, **46**, 644 (2008).
71. D. Hua, H. H. Yi, X. L. Tang, Q. F. Yu, P. Ning and L. P. Yang, *Chem. Eng. J.*, **188**, 77 (2012).
72. H. Y. Hu, T. W. Zhang, J. D. Wiggins-Camacho, G. S. Ellis, M. D. Lewan and X. L. Zhang, *Mar. Pet. Geol.*, **59**, 114 (2015).
73. B. Zhang, L. Y. Luan, R. T. Gao, F. Li, Y. J. Li and T. Wu, *Colloids Surf. A*, **520**, 399 (2017).

Supporting Information

Preparation of nano-sized Mg-doped copper silicate materials using coal gangue as the raw material and its characterization for CO_2 adsorption

Yu Wu[*,], Zhaojun Wu[*,**], Kai Liu[*,**], Fu Li[*,**], Yujie Pang[*,**], Jianbin Zhang[*,**,†], and Huayan Si[**,***,†]**

*College of Chemical Engineering, Inner Mongolia University of Technology, Hohhot 010051, China
**Inner Mongolia Engineering Research Center for CO_2 Capture and Utilization, Hohhot 010051, China
***School of Materials Science and Engineering, Hebei Provincial Key Laboratory of Traffic Engineering materials, Shijiazhuang Tiedao University, Shijiazhuang 050043, China
(*Received 29 March 2020 • Revised 17 May 2020 • Accepted 27 May 2020*)

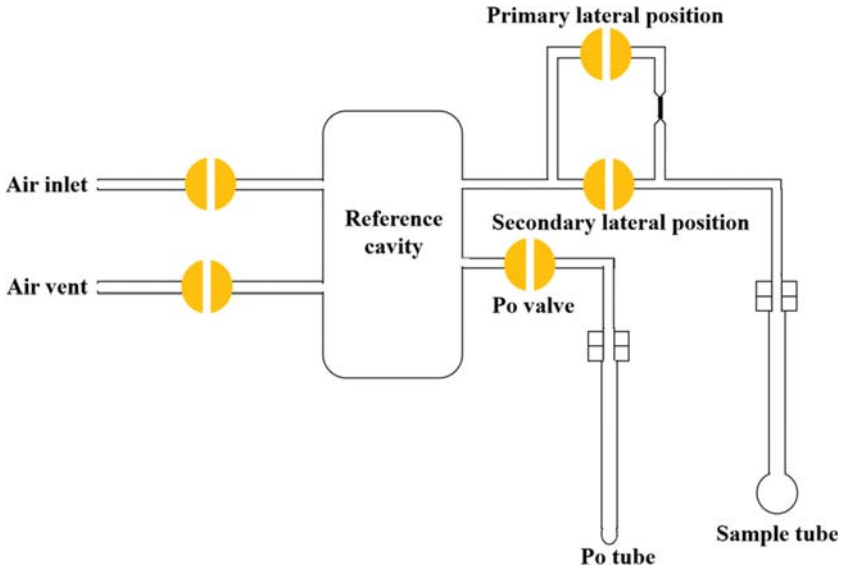

Fig. S1. Schematic diagram of the experimental setup for sample adsorption of CO_2.

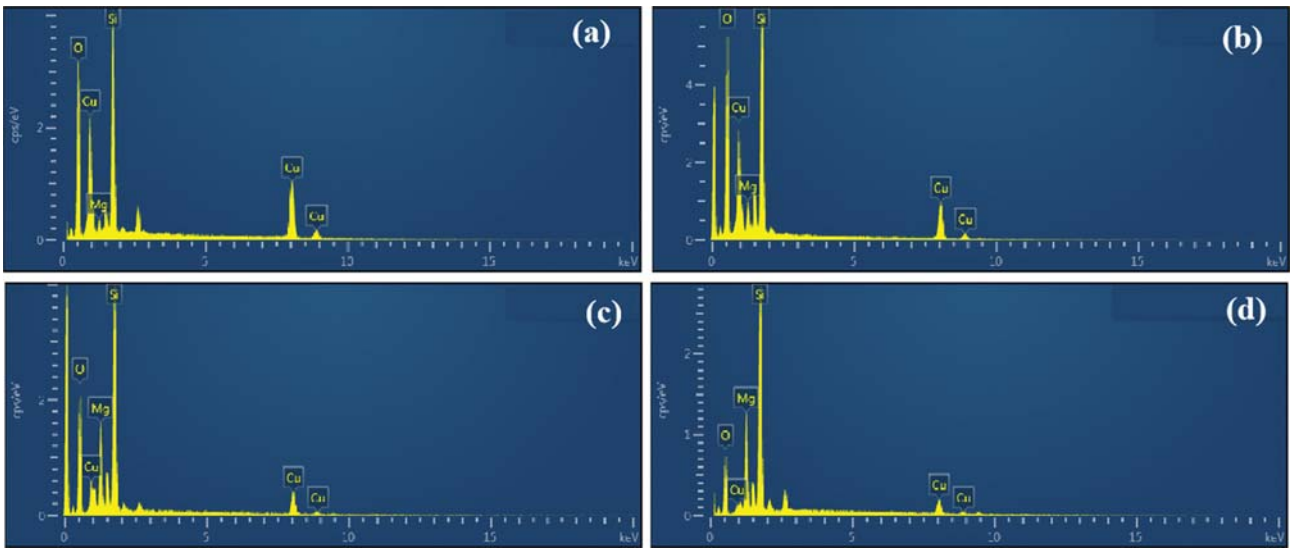

Fig. S2. Energy spectra of $Mg_{0.25}$-$Cu_{0.75}$-SiO_3 (a), $Mg_{0.5}$-$Cu_{0.5}$-SiO_3 (b), $Mg_{0.75}$-$Cu_{0.25}$-SiO_3 (c), $Mg_{0.9}$-$Cu_{0.1}$-SiO_3 (d).

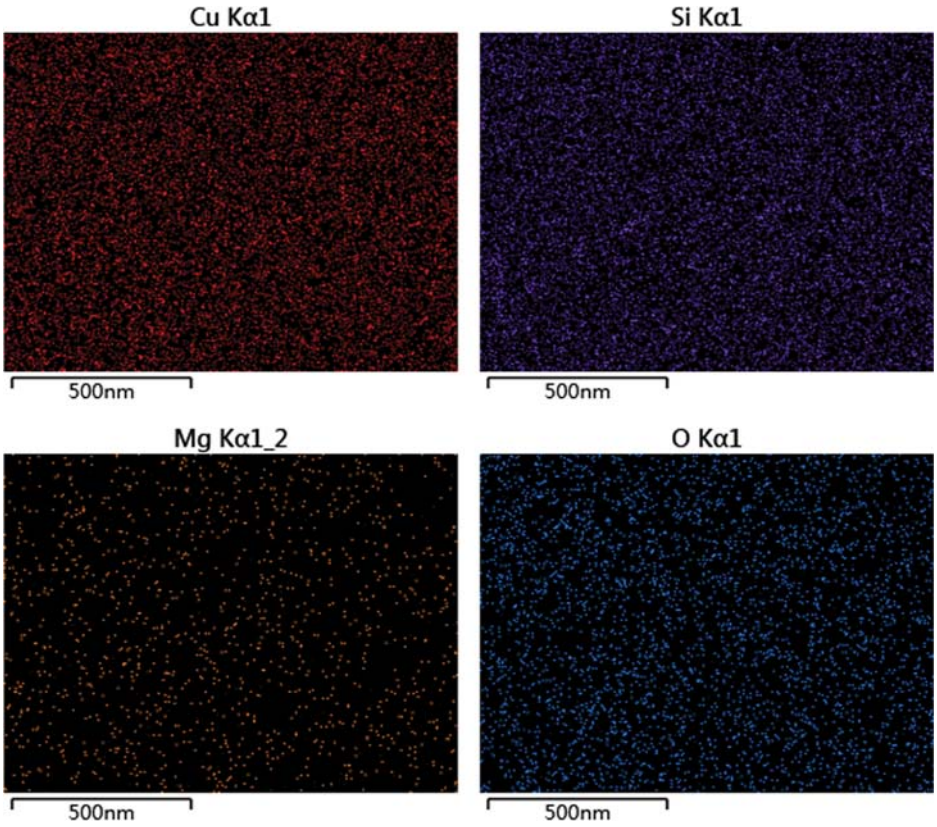

Fig. S3. EDS mapping of Cu, Si, Mg, and O elements in $Mg_{0.25}$-$Cu_{0.75}$-SiO_3.

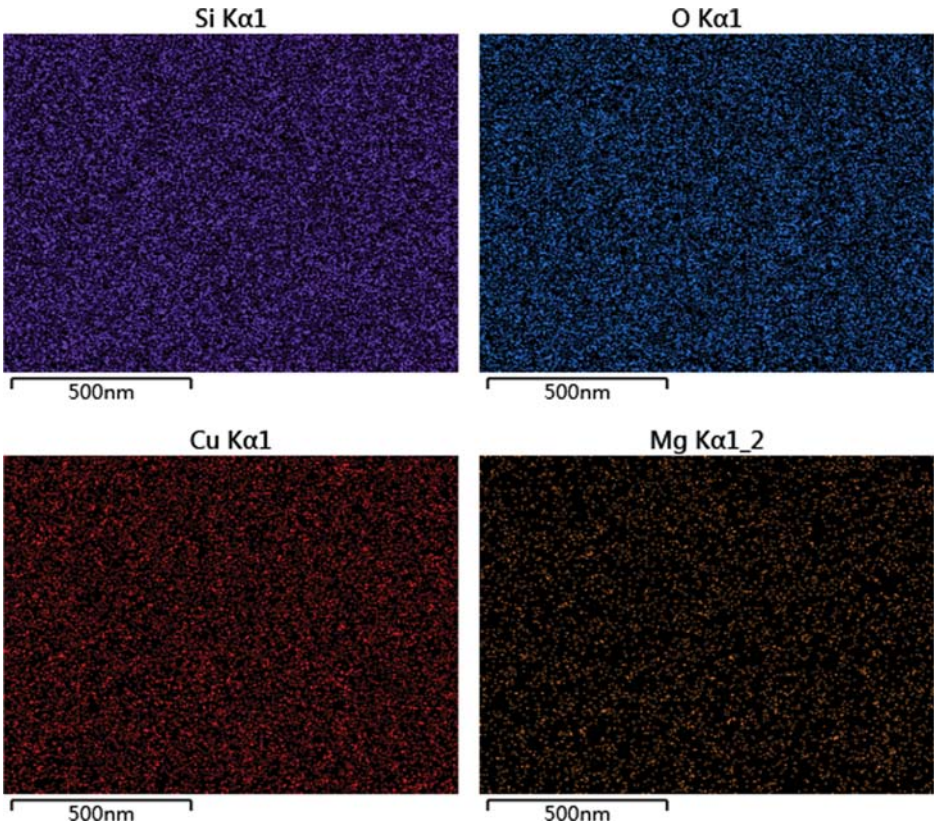

Fig. S4. EDS mapping of Cu, Si, Mg, and O elements in $Mg_{0.5}$-$Cu_{0.5}$-SiO_3.

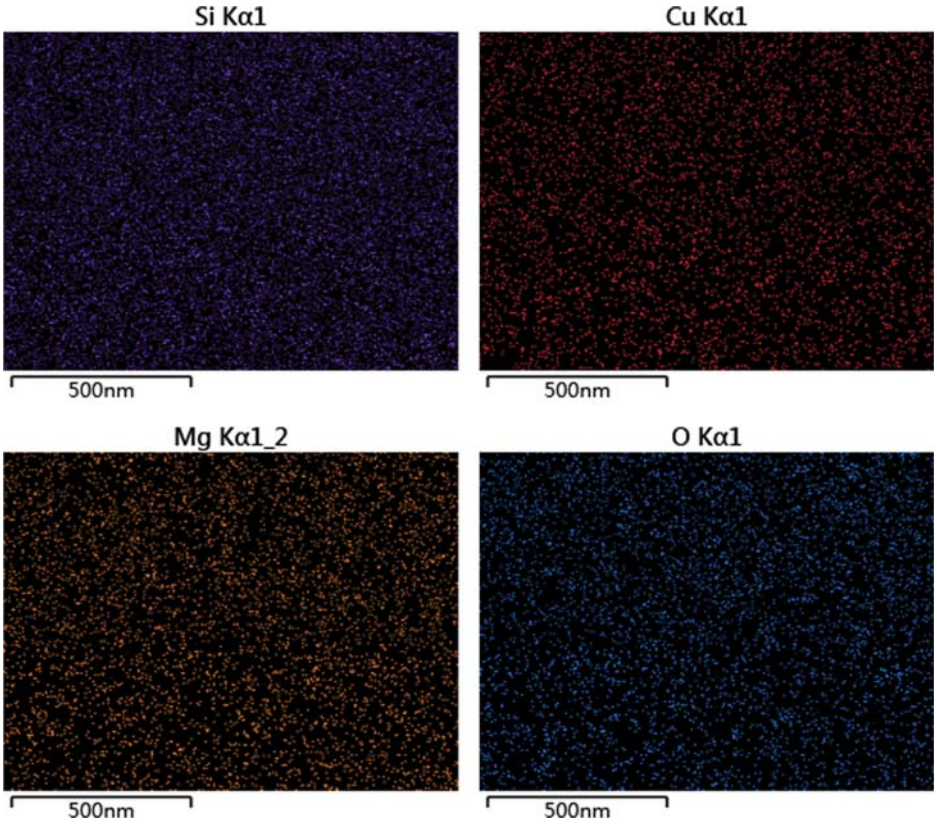

Fig. S5. EDS mapping of Cu, Si, Mg, and O elements in $Mg_{0.75}$-$Cu_{0.25}$-SiO_3.

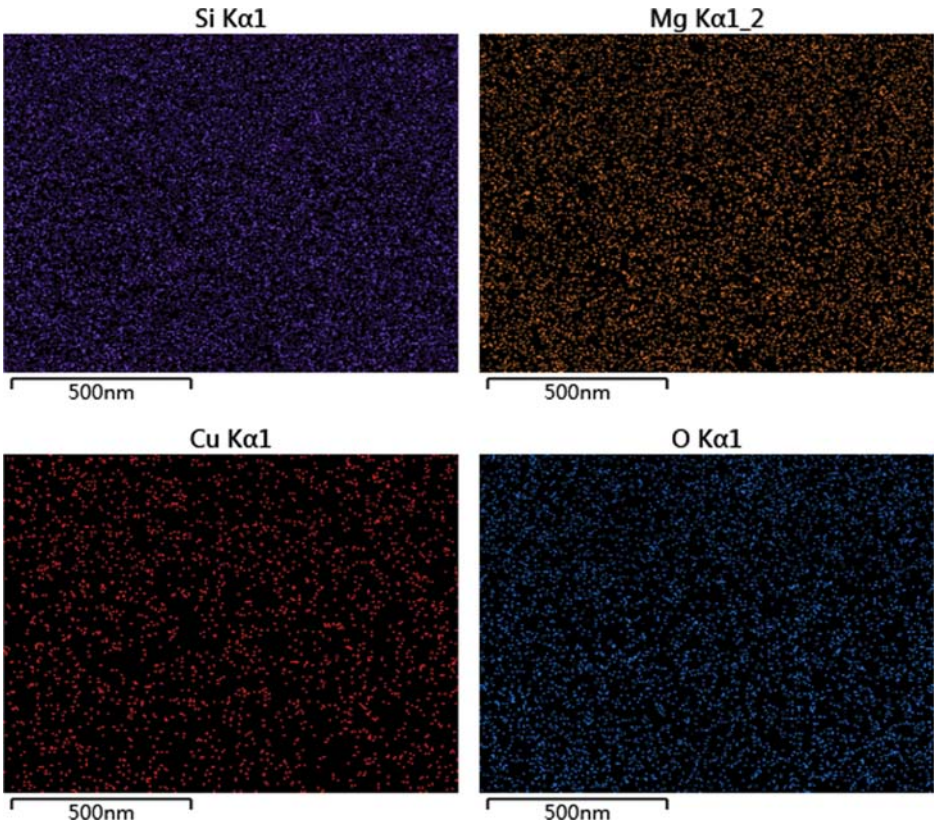

Fig. S6. EDS mapping of Cu, Si, Mg, and O elements in $Mg_{0.9}$-$Cu_{0.1}$-SiO_3.

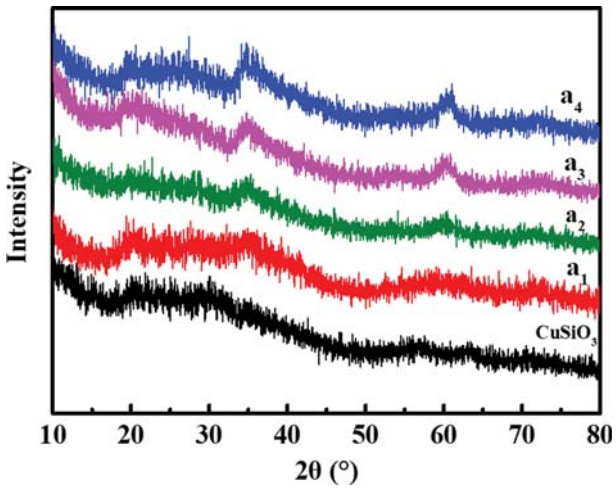

Fig. S7. XRD patterns of Mg_x-Cu_{1-x}-SiO_3 (a_1: $Mg_{0.25}$-$Cu_{0.75}$-SiO_3; a_2: $Mg_{0.5}$-$Cu_{0.5}$-SiO_3; a_3: $Mg_{0.75}$-$Cu_{0.25}$-SiO_3; a_4: $Mn_{0.9}$-$Cu_{0.1}$-SiO_3).